

# An Analytical Solution for the Initiation and Early Progression of Fretting Wear in Spherical Contacts

**Huaidong Yang**

G. W. Woodruff School of Mechanical Engineering,  
Georgia Institute of Technology,  
Atlanta, GA 30332  
e-mail: yanghuaidong@gatech.edu

**Itzhak Green<sup>1</sup>**

Fellow ASME  
G. W. Woodruff School of Mechanical Engineering,  
Georgia Institute of Technology,  
Atlanta, GA 30332  
e-mails: green@gatech.edu;  
itzhak.green@me.gatech.edu

*This article derives analytical solutions to calculate the wear volume at the initiation of fretting motion and its early progression over the first few oscillation cycles. The Archard-based model considers a deformable hemisphere that is contact with a deformable flat block. The material pairs investigated are special alloys, the Inconel 617/Incoloy 800H, and Inconel 617/Inconel 617. The analytical study begins with a unidirectional frictional sliding contact, where the local interfacial sliding distance and the nominal sliding distance at the initiation of gross slip are derived. The obtained analytical expressions for unidirectional sliding are then used to derive the corresponding wear volume for the initiation and early progression of gross slip and the wear volume for a general fretting cycle under elastic conditions. These analytical derivations are all verified by the finite element analysis (FEA). The FEA method and the analytical solutions render virtually identical results for both similar and dissimilar material pairs. The effects of plasticity on the wear volume under elastic–plastic conditions are also investigated. It is found that the fretting wear volumes obtained from the FEA simulations, which include plasticity, are close to those obtained from the analytical expressions for purely elastic regimes. All the results are presented in normalized forms, which can be easily generalized and applied to three-dimensional fretting wear of other material pairs. [DOI: 10.1115/1.4051585]*

*Keywords:* contact mechanics, friction, sliding, surfaces, wear, fretting

## 1 Introduction

This study is directly related to components used in high-temperature gas cooled reactors (HTGRs) (800 °C) and very high-temperature gas cooled nuclear reactors (850 °C and above) (VHTRs). In particular, valve stems and seats, control rod drive mechanisms, fuel handling mechanisms, and helium circulators suffer from fretting wear that can significantly reduce the operational lifetime of these components. Alloy 800H and Inconel 617 are promising structural materials that possess excellent high-temperature strength, while resisting corrosion and oxidation. They are specifically envisaged for use in such reactors, and hence, they are the target materials in the current investigation.

Frictional sliding institutes the underlying mechanism for fretting wear. Johnson, in his book [1], provides fundamental solutions for surface deformation of half elastic spaces subject to a Hertzian contact pressure and a proportional traction (via a constant coefficient of friction) considering two configurations, cylindrical and spherical contacts. The solution for the spherical contact will be used herein to build the three-dimensional (3D) fretting wear model.

One of the very first investigations regarding fretting is that by Tomlinson et al. [2], where the terminology “fretting corrosion” was coined. Subsequently, Vingsbo and Söderberg [3] established a fretting map, which sorts fretting into stick, mixed stick-slip, and gross slip regimes. Under a certain normal load, the contact status transitions from stick to partial slip and gross slip with the increase of the tangential displacement. A mixed fretting regime is identified from the fretting loop evolution by Zhou and Vincent [4,5], showing a shape that varies during thousands of fretting cyclic loadings.

Fretting wear is the main cause of component failure in the gross slip regime. It is investigated by Waterhouse [6], McColl et al. [7], Fouvry et al. [8], and Blanchard et al. [9]. Two recognized models are used in the study of fretting wear, the Archard wear model, and the accumulated dissipated energy model. The Archard wear model is more conducive for numerical implementation, and its use is quite prevalent in such studies. For example, McColl et al. [7] and Ding et al. [10] study the fretting wear in cylindrical contacts, while Ratsimba et al. [11] study the fretting wear in spherical contacts. These works use the commercial finite element analysis (FEA) software, ABAQUS, to apply the Archard wear model at the interface and update the contact profile during the fretting motion. Conversely, the accumulated dissipated energy model is more prevalent in experimental works. Fridrici et al. [12] and Fouvry et al. [8] interpret the wear volume during their fretting experiments through the accumulated dissipated energy model. Paulin et al. [13] also apply the accumulated dissipated energy model to the finite element model to study the evolution of surface wear. However, none of the aforementioned works produce analytical expressions for the wear volume with respect to material properties and loading conditions. In addition, all their loading conditions are purely elastic, neglecting elastic–plastic conditions.

The elastic–plastic and fully plastic spherical contacts in strictly normal loading have been studied in great details using the FEA method [14–16]. Analytical solutions to the threshold conditions of plasticity onset in spherical and cylindrical contacts are given by Green [17]. The elastic–plastic fretting contact is also studied using the finite element method in both the cylindrical [18,19] and spherical contacts [20]. None of these analyses incorporates wear.

In the current study, a 3D fretting wear model is developed for a deformable hemisphere in contact with a deformable flat block. The Archard wear model is applied at the interface. Closed-form analytical solutions are derived to calculate the wear volume for frictional sliding in a purely elastic 3D contact at the initiation of gross slip

<sup>1</sup>Corresponding author.

Contributed by the Tribology Division of ASME for publication in the JOURNAL OF TRIBOLOGY. Manuscript received February 19, 2021; final manuscript received June 21, 2021; published online July 22, 2021. Assoc. Editor: Yong Hoon Jang.

and then for one general cycle. A corresponding finite element code is employed to model the fretting wear using the commercial code ANSYS. The results obtained from the analytical solutions are then compared with those obtained from FEA, where their very good agreements mutually verify both the analytical solutions and the FEA results. In addition, the fretting contact in the elastic–plastic regime is also studied by the finite element method, and the effect of plasticity on the wear volume is investigated and compared to the solutions for the purely elastic regime.

While a two-dimensional (2D) cylindrical contact fretting wear study has been done in Ref. [21], this study offers the theoretical and numerical studies of fretting wear for 3D hemispherical contacts. All the results are presented in normalized forms. Hence, while this study concentrates on Alloys 800H and 617, the dimensionless results can easily be generalized and applied to 3D fretting wear of different material pairs. The derived solutions for the wear volume in the current work do not consider changes in the contact geometry during the fretting motion. Consequently, the analytical results may be applicable only for the initial few cycles of fretting. Likewise, because of the heavily burdened computational efforts, the FEA results are done for up to three cycles of fretting motion.

## 2 Fretting Wear Model

The fretting wear model is developed for an oscillating deformable hemisphere of radius  $R$  and a stationary deformable flat block, as shown in Fig. 1(a). Because of the symmetry, the hemisphere and the block are cut in half along the  $XZ$  vertical plane. A rigid plate is placed on the top surface of the hemisphere to preserve a uniform downward displacement along that plane. The interface between the upper rigid plate and the hemisphere is set to be frictionless, as indicated in Fig. 1(b). The external normal load,  $P$ , is applied to the top surface of that rigid plate (which is allowed to have a vertical motion only), while the reciprocal displacement,  $\delta$ , is applied at the top surface of the hemisphere along the  $X$ -direction. The interference,  $\omega$ , and the tangential force,  $Q$ , are outputs.

For the FEA model, roller boundary conditions of no displacement normal to the plane are applied to the vertically cut plane of the quarter sphere (enforcing the symmetry with respect to the  $XZ$  plane) and to all of the five faces of the block, except to the block top face (the  $XY$  plane), which is free to deform in all directions.

The materials of the hemisphere and the bottom flat block are first set to be an identical material pair, Inconel 617/Inconel 617. Then, the materials are set to be dissimilar, Inconel 617/Incoloy 800H. The designation of Inconel 617/Incoloy 800H means that the material of the hemisphere is Inconel 617 and that of the block is Incoloy 800H. As indicated, these special alloys are promising materials for the structural and in-core components of HTGRs/VHTRs. The material properties are listed in Table 1 (the parameter  $C(\nu)$  and the product  $C(\nu) \cdot S_y$  are explained in this study).

The Archard wear model [23] is used at the contact between the hemisphere and the flat block:

$$V = \frac{KPS}{H} \quad (1)$$

where  $V$ ,  $K$ ,  $P$ ,  $S$ , and  $H$  represent the wear volume, the dimensionless wear coefficient, the normal force, the sliding distance, and the hardness of the softer material, respectively. The hardness is assumed to be  $H = 2.8S_y$ .<sup>2</sup> The wear coefficient is set to  $10^{-5}$  without loss of generality.<sup>3</sup> The details of how the Archard wear

model is implemented in a 2D cylindrical contact are given in Ref. [21]. Here, however, for a 3D model, the Archard wear model is applied locally (i.e., at each nodal point) at the contact region.

**2.1 Theoretical Equations for Normal Contact.** In the regime of static elastic normal contact, the Hertzian theory gives the solution to the 3D spherical contact [1]. The relations among the normal load,  $P$ , the contact radius,  $a$ , the maximum contact pressure,  $p_0$ , the interference,  $\omega$ , and the pressure distribution,  $p(r)$  are given by

$$a = \left( \frac{3PR}{4E'} \right)^{\frac{1}{3}} \quad (2)$$

$$p_0 = \frac{3P}{2\pi a^2} \quad (3)$$

$$\omega = \left( \frac{\pi p_0}{2E'} \right)^2 R \quad (4)$$

$$p(r) = p_0 \left( 1 - \frac{r^2}{a^2} \right)^{\frac{1}{2}} \quad (5)$$

where  $E'$  is the equivalent elastic modulus:

$$\frac{1}{E'} = \frac{1 - \nu_1^2}{E_1} + \frac{1 - \nu_2^2}{E_2} \quad (6)$$

In normal elastic contacts, Green [17] defined the ratio between the maximum pressure and the maximum von Mises stress to be  $C = p_0/\sigma_{e-max}$ , which is solely dependent on Poisson's ratio. A curve-fit expression is rendered for 3D contacts,  $C(\nu) = 1.30075 + 0.87825\nu + 0.54373\nu^2$ . At yielding by definition  $\sigma_{e-max} = S_y$ , such that the product  $CS_y$  gives the corresponding maximum pressure,  $p_0$ , at yielding onset. For dissimilar materials (as is one case herein), Green [17] teaches that the effective product is determined by  $CS_y = \min(C(\nu_1)S_{y1}, C(\nu_2)S_{y2})$ . Likewise, the critical contact radius,  $a_c$ , the critical load,  $P_c$ , and the critical interference,  $\omega_c$ , are also derived as follows [17]:

$$a_c = \frac{\pi CS_y R}{2E'} \quad (7)$$

$$P_c = \frac{(\pi CS_y)^3 R^2}{6E'^2} \quad (8)$$

$$\omega_c = \left( \frac{\pi CS_y}{2E'} \right)^2 R \quad (9)$$

Note that the product  $CS_y$  appears as a single-term entity in these critical values.

By substituting the material properties in Table 1 into Eqs. (7)–(9), the said critical parameters are calculated and are listed in Table 2. The critical contact area is calculated based on  $a_c$ ,  $A_c = \pi a_c^2$ . These critical values are subsequently used to normalize (i.e., generalize) the results of this work.

**2.2 Theoretical Equations for Tangential Contact.** To assess the effect of traction, a constant friction of coefficient (COF)<sup>4</sup>,  $\mu$ , is applied to the interface. For a tangential force,  $Q < \mu P$ , the interface experiences partial-slip conditions. As shown

<sup>2</sup>Equation (1) is used as Archard intended, regarding hardness as a material property. According to the work by Jackson and Green [15], it has been shown that hardness actually depends not only on the yield strength but also on the deformation. For consistency with the Archard original model, however, hardness is used here as if it were a constant material property.

<sup>3</sup>Results will be nondimensionalized, but a numerical value is needed for the FEA numerical execution.

<sup>4</sup>A constant friction coefficient is not a limitation of the finite element model used herein. A varying COF can straightforwardly be applied in the computer code. However, for analysis, it is convenient to control some parameters, one of which is the COF.

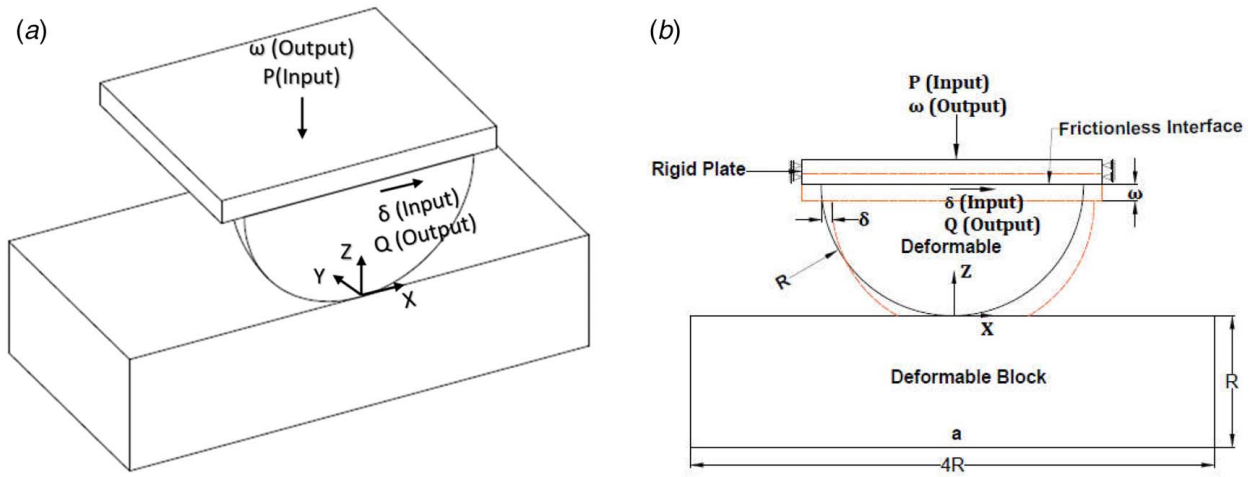


Fig. 1 Schematic of a quarter sphere in contact with a flat block for a force-controlled model: (a) 3D view and (b) front view

Table 1 The material properties and critical values for two cases [22]

Temperature	Material	Elastic modulus (GPa) $E$	Yield strength (MPa) $S_y$	Poisson's ratio $\nu$	$C(\nu)$	$C \cdot S_y$ (MPa)
20 °C	Inconel 617	211.0	322	0.3	1.615	520
20 °C	Incoloy 800H	196.5	150	0.339	1.662	249

schematically in Fig. 2, within the contacting region ( $-a < x < a$ ), the conditions are stick for  $[-c, c]$  and slip between  $[-a, -c]$   $U$   $[c, a]$ . The parameter,  $c$ , is called the stick half-width.

According to Johnson [1], the tangential traction within the slip region,  $q'(r)$ , and the complementary tangential traction within the stick region,  $q''(r)$ , for an half elastic space are given by:

$$q'(r) = \mu p_0 \left(1 - \frac{r^2}{a^2}\right)^{\frac{1}{2}} \quad r \leq a \quad (10)$$

$$q''(r) = -\frac{c}{a} \mu p_0 \left(1 - \frac{r^2}{c^2}\right)^{\frac{1}{2}} \quad r \leq c \quad (11)$$

As shown in Fig. 2, the tangential traction in the slip region is  $q(r) = q'(r)$ , and the tangential traction in the stick region is  $q(r) = q'(r) + q''(r)$ . With the increase of the tangential displacement,  $\delta$ , and with it the tangential force,  $Q$ , the stick region decreases. When  $Q = \mu P$ , the stick region vanishes,  $c = 0$ , which means that gross slip initiates. Assuming  $X$  to represent the direction of sliding motion, the tangential displacement at the surface of contact in that direction is  $\bar{u}_x(x, y)$ , which is also given by Johnson [1]:

$$\bar{u}_x = \frac{\pi \mu p_0}{32 G a} [4(2 - \nu)a^2 + (4 - \nu)x^2 + (4 - 3\nu)y^2] \text{sgn}(q(x, y)) \quad (12)$$

where  $G$  is the shear modulus of the material, and it can be obtained for each material by:

$$G = \frac{E}{2(1 + \nu)} \quad (13)$$

Referring to the coordinates shown in Fig. 1, when the hemisphere is forced in the positive  $X$ -direction, the tangential force it experiences should be  $-q'(r)$ , as given by Eq. (10). The corresponding tangential force that the block experiences is therefore  $+q'(r)$ . The substitution of Eq. (10) into Eq. (12) yields the corresponding tangential displacements at the surface of the contact,  $\bar{u}_{x1}(x)$ , on the hemisphere, and  $\bar{u}_{x2}(x)$ , on the block, respectively:

$$\bar{u}_{x1} = -\frac{\pi \mu p_0}{32 G_1 a} [4(2 - \nu_1)a^2 + (4 - \nu_1)x^2 + (4 - 3\nu_1)y^2] \quad r \leq a \quad (14)$$

$$\bar{u}_{x2} = \frac{\pi \mu p_0}{32 G_2 a} [4(2 - \nu_2)a^2 + (4 - \nu_2)x^2 + (4 - 3\nu_2)y^2] \quad r \leq a \quad (15)$$

where  $\bar{u}_{x1}(0, 0)$  represents the sliding distance of the last stick point relative to the hemisphere bulk body, while  $\bar{u}_{x2}(0, 0)$  represents the sliding distance of the last stick point relative to the bottom block bulk body. It is now possible to obtain the local relative sliding distance between the hemisphere and the flat block at the initiation of gross slip by

$$s_0(x, y) = [\bar{u}_{x1}(0, 0) - \bar{u}_{x1}(x, y)] + [\bar{u}_{x2}(x, y) - \bar{u}_{x2}(0, 0)] \quad (16)$$

The substitution of  $\bar{u}_{x1}$  and  $\bar{u}_{x2}$  of Eqs. (14) and (15) into Eq. (16) results in

$$s_0(x, y) = \frac{\pi \mu p_0}{32 G_1 a} [(4 - \nu_1)x^2 + (4 - 3\nu_1)y^2] + \frac{\pi \mu p_0}{32 G_2 a} [(4 - \nu_2)x^2 + (4 - 3\nu_2)y^2] \quad (17)$$

Table 2 The critical values (onset of plasticity) for different material schemes

Temperature	Hemisphere material	Block material	Critical interference $\omega_c$ ( $\mu\text{m}$ )	Critical load $P_c$ (kN)	Critical contact radius $a_c$ (mm)	Critical contact area $A_c$ ( $\text{mm}^2$ )
20 °C	Inconel 617	Inconel 617	24.8	13.472	3.52	38.9
20 °C	Inconel 617	Incoloy 800H	5.96	1.556	1.73	9.36

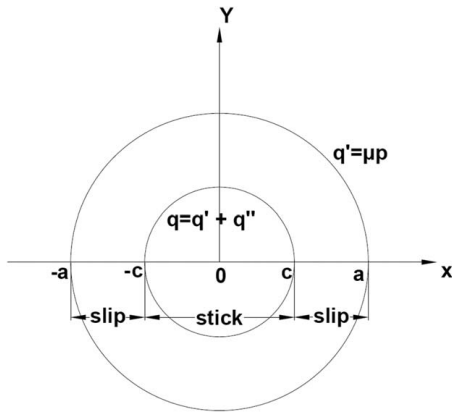


Fig. 2 The distribution of tangential surface traction of the spherical contact under a tangential force,  $Q < \mu P$

For identical material pairs, using the relations,  $E = E_1 = E_2$  and  $\nu = \nu_1 = \nu_2$ , Eq. (17) simplifies to

$$s_0(x, y) = \frac{\pi \mu p_0}{16 G a} [(4 - \nu)x^2 + (4 - 3\nu)y^2] \quad (18)$$

It is again emphasized that these initial gross slip equations, in Eqs. (17) and (18), are derived for purely elastic conditions.

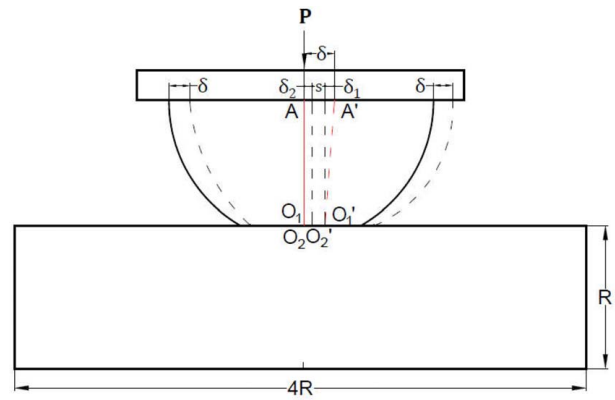


Fig. 3 The schematic of the sliding distance for the front view of the model

The mesh convergence for the current finite element model is not discussed herein. First, the mesh convergence detail for the pure normal contact is given in Ref. [20], and for brevity, that convergence analysis applies here just as well, and thus, it is not repeated. Second, the results from the analytical solution and those from the finite element method are compared in the next sections. Because of their very good agreement (which is forthcoming), it obliges yet another confirmation of the FEA model convergence.

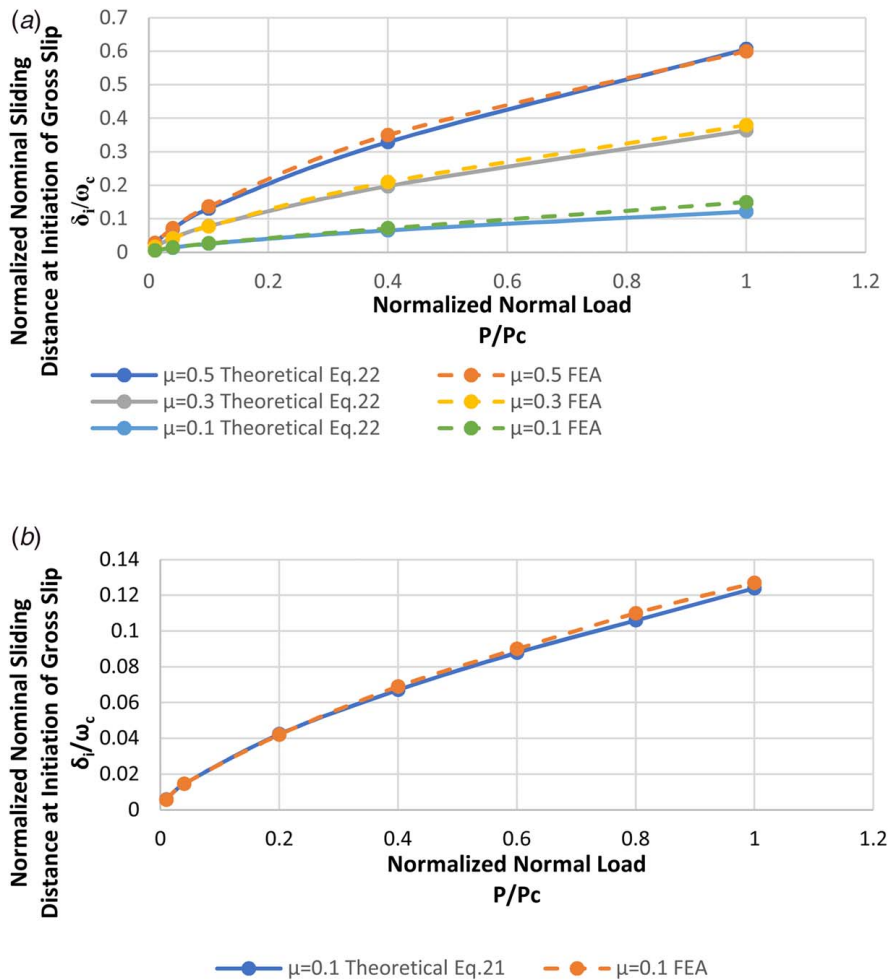


Fig. 4 The dimensionless nominal sliding distance at the initiation of gross slip under different normal loads with (a)  $\mu = 0.1, 0.3$ , and  $0.5$  (bottom to top curves, respectively) for the FEA results and Eq. (22) results for Inconel 617/Inconel 617 and (b)  $\mu = 0.1$  for the FEA results and Eq. (21) results for Inconel 617/Incoloy 800H

### 3 The Analytical Solution and Results Comparison With the Finite Element Analysis Model

**3.1 The Nominal Sliding Distance at Initiation of Gross Slip.** We distinguish between a few terms used in this study regarding positioning. These include the nominal sliding distance,  $\delta$ , the interfacial sliding distance,  $s$ , the deformation on the hemisphere,  $\delta_1$ , and the deformation on the flat block,  $\delta_2$ . The schematic of contact is shown in Fig. 3. When a nominal sliding distance  $\delta$  is applied to the top surface of the hemisphere uniformly, the centerline of the hemisphere deforms from  $O_1A$  to  $O_1'A'$ , while the center of the contact on the block displaces from  $O_2$  to  $O_2'$ . As shown in the schematic of Fig. 3, the nominal sliding distance,  $\delta$ , equals to the sum of the deformation on the hemisphere,  $\delta_1$ , the local interfacial sliding distance at the center of contact  $s(r=0)$ , and the deformation on the flat block,  $\delta_2$ .

At the initiation of gross slip, the tangential force is  $Q = \mu P$ , and the local interfacial sliding distance at the center of contact is  $s(r=0) = 0$ . The corresponding deformation of the two bodies can be estimated by assuming two elastic half-spaces under a Hertzian pressure and a tangential traction of  $\mu P$  imbedded in Eqs. (14) and (15), such that

$$\delta_{i1} = \bar{u}_{x1}(0, 0) = \frac{\pi \mu p_0}{32 G_1 a} [4(2 - \nu_1) a^2] \quad (19)$$

$$\delta_{i2} = \bar{u}_{x2}(0, 0) = \frac{\pi \mu p_0}{32 G_2 a} [4(2 - \nu_2) a^2] \quad (20)$$

By adding  $\delta_{i1}$  and  $\delta_{i2}$  and substituting Eq. (6), the nominal sliding distance at the initiation of gross slip is derived as follows:

$$\delta_i = \frac{3 \mu P}{8 a} \left[ \frac{(2 - \nu_1)(1 + \nu_1)}{E_1} + \frac{(2 - \nu_2)(1 + \nu_2)}{E_2} \right] \quad (21)$$

For identical material pairs, Eq. (21) can be further simplified to give:

$$\delta_i = \frac{3(2 - \nu)(1 + \nu) \mu P}{4 E a} \quad (22)$$

Figure 4(a) shows the dimensional nominal sliding distance at the initiation of gross slip under different normal loads with COFs of  $\mu = 0.1, 0.3, \text{ and } 0.5$  for Inconel 617/Inconel 617, and Fig. 4(b) shows the corresponding results for  $\mu = 0.1$  for Inconel 617/Incoloy 800H. The normal load ranges from  $0.01 P_c$  to  $1 P_c$ . The results from the FEA and Eqs. (21) and (22) agree well with less than 5% difference in the entire range. The very good agreement between FEA results and theoretical predictions for both similar and dissimilar contact pairs mutually substantiates the equations derived in Eqs. (21) and (22), and the FEA model alike.

**3.2 The Wear Volume at Initiation of Gross Sliding.** Caused by the tangential displacement,  $\delta$ , as the tangential force  $Q$  increases from 0 to  $\mu P$ , the partial-stick, partial-slip condition applies to the contact. The local wear volume per unit area,  $v(x, y)$ , according to the Archard wear model, is calculated locally at the interface by

$$v(x, y) = \frac{K}{H} p(x, y) s_x(x, y) \quad (23)$$

That is governed by the dimensionless wear coefficient,  $K$ , the contact pressure,  $p(x, y)$ , the local interfacial sliding distance,  $s_x(x, y)$ , and the hardness of the wearing body,  $H$ . At the onset of gross sliding,  $s_x(x, y) = s_0(x, y)$ , as given by Eq. (17) (or Eq. (18) for identical material pairs). Substituting  $s_0(x, y)$  and Hertzian pressure,  $p(r)$ , into Eq. (23), the total wear volume at the inception of gross sliding,  $V_0$ , can be integrated over the area of contact:

$$\begin{aligned} V_0 &= \int_0^a \int_0^{2\pi} \frac{K}{H} p(r, \theta) s_0(r, \theta) r d\theta dr \\ &= \int_0^a \int_0^{2\pi} \frac{K \mu \pi p_0^2 \sqrt{1 - \frac{r^2}{a^2}}}{32 a H} \left[ \frac{(4 - \nu_1) r^2 \cos^2 \theta + (4 - 3\nu_1) r^2 \sin^2 \theta}{G_1} + \frac{(4 - \nu_2) r^2 \cos^2 \theta + (4 - 3\nu_2) r^2 \sin^2 \theta}{G_2} \right] r d\theta dr \\ &= \frac{K \pi^2 \mu p_0^2 a^3}{60 H} \left( \frac{2 - \nu_1}{G_1} + \frac{2 - \nu_2}{G_2} \right) \end{aligned} \quad (24)$$

For the identical material pair, the wear volume at the initiation of gross slip is expressed as follows:

$$V_0 = \frac{K \pi^2 \mu p_0^2 a^3 (2 - \nu)}{30 H G} \quad (25)$$

To normalize the results, a critical wear volume,  $V_c$ , is now defined as follows:

$$V_c = \frac{K_c \omega_c P_c}{H} \quad (26)$$

Herein, the critical wear coefficient is set by definition to be  $K_c = 1$ . Figure 5(a) shows the wear volume at the initiation of gross slip,  $V_0$ , for  $\mu = 0.1, 0.3, \text{ and } 0.5$  for Inconel 617/Inconel 617, and Fig. 5(b) shows the corresponding results for  $\mu = 0.1$  for Inconel 617/Incoloy 800H. The normal load for each material ranges from  $0.01 \times P_c$  to  $1 \times P_c$ . The results for the three cases from the FEA and Eqs. (24) and (25) are all in excellent agreement with less than 5% difference, which supports the viability of using Eqs. (24) and (25) for different material pairs.

**3.3 Prediction of Fretting Wear Volume Under Elastic Conditions.** First, a pure normal contact is applied bringing the hemisphere into an interference contact with the block, deforming both. Then frictional fretting cycling ensues. One complete fretting cycle is separated into four unidirectional strokes imposed on the hemisphere at the interface with the rigid plate. Starting motion from an origin (say, point A in Fig. 3), the first stroke is in the positive  $X$ -direction completing a certain predetermined amplitude,  $\Delta$ . It is then followed by a return stroke to the origin in the negative  $X$ -direction. The next stroke continues in the negative  $X$ -direction having the same amplitude. The last stroke happens in the positive  $X$ -direction returning the rigid plate back to its origin. The details can be found in the 2D work [21]. The oscillation amplitude of the fretting cycle is symbolized as  $\Delta$ . For fretting that experiences gross slip condition ( $\delta_i < \Delta$ ), the total wear volume for a general cycle of fretting during partial-slip condition is then:

$$V_{\text{partial}} = 4V_0 \quad \delta_i < \Delta \quad (27)$$

The total nominal sliding distance for the gross slip condition during a general cycle is  $\Delta S = 4(\Delta - \delta_i)$ . Hence, the corresponding

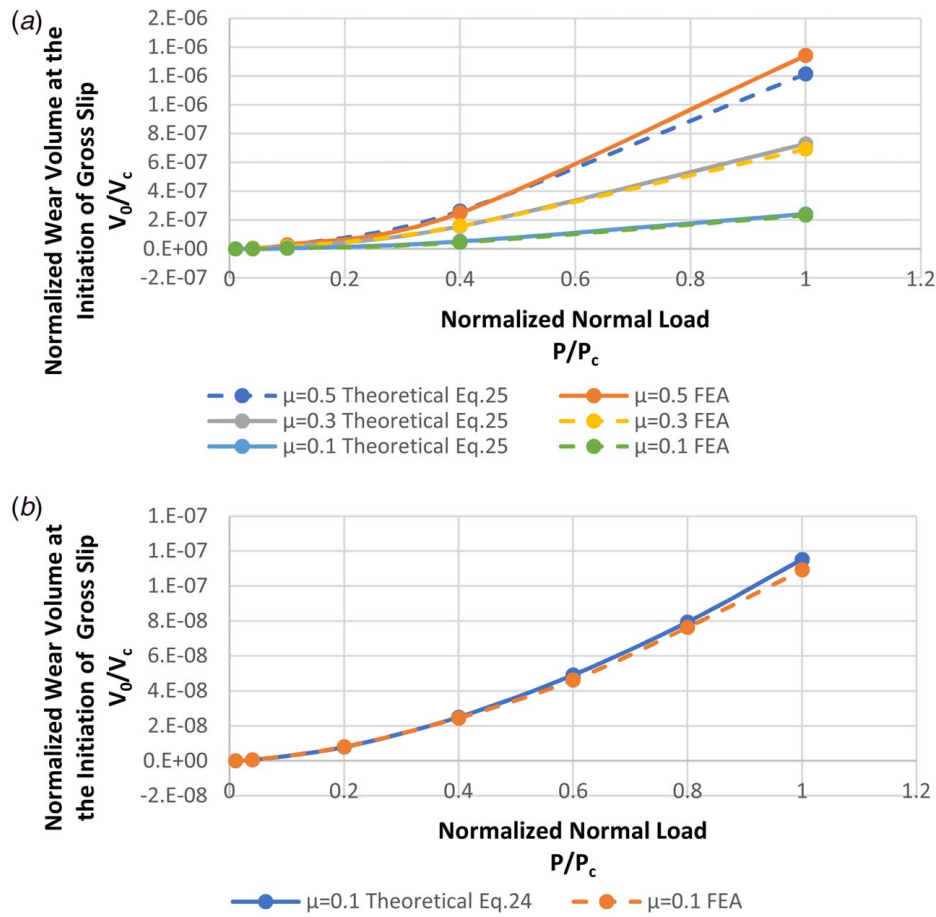


**Fig. 5** The normalized wear volume at the initiation of gross slip,  $V_0$ , (a) from FEA and Eq. (25) at different normal loads with  $\mu = 0.1, 0.3$ , and  $0.5$  (bottom to top curves, respectively) for Inconel 617/Inconel 617 and (b) from FEA and Eq. (24) at different normal loads with  $\mu = 0.1$  for Inconel 617/Incoloy 800H

wear volume for gross slip is expressed as follows:

$$V_{\text{slip}} = \frac{4(\Delta - \delta_i)KP}{H} \quad \delta_i < \Delta \quad (28)$$

Adding  $V_{\text{partial}}$  and  $V_{\text{slip}}$  yields the wear volume for a general cycle of the fretting motion:

$$V = 4V_0 + \frac{4(\Delta - \delta_i)KP}{H} \quad \delta_i < \Delta \quad (29)$$

When  $\delta_i > \Delta$ , the partial-slip condition is sustained for the whole cycle. That results in a small and mostly negligible wear volume. For the following results for both analytical and numerical solutions, the oscillation amplitude is set to  $\Delta = \omega_c$  for each case.

Figure 6(a) shows the results of the wear volume for one cycle of fretting motion under elastic condition for  $\mu = 0.1, 0.3$ , and  $0.5$  under different normal loads for Inconel 617/Inconel 617, and Fig. 6(b) shows the corresponding results for  $\mu = 0.1$  for Inconel 617/Incoloy 800H. The results from the FEA and those from theory, as derived earlier, are yet again in very good agreement, such that they mutually verify each other. Note that while the FEA results are obtained for half domains (symmetry planes are used to reduce computation times), the results reflect the total wear volumes. The difference is a bit larger with larger COFs, which is caused by the “beam” deformation effect (i.e., that of the hemisphere). When the COF is large, the friction force is also large, which causes the deformations of the hemisphere and the block to act as two beams. As a result, the deformation decreases the actual local interfacial sliding distance.

**3.4 Comparison of Wear for the Material Pairs.** Concerning practical matters, the wear volumes on the hemisphere and the block are now compared in Fig. 7 between the two schemes of material pairs (see Table 2) Inconel 617/Inconel 617 and Inconel 617/Incoloy 800H, for a general cycle of fretting motion under the same loading parameters, which are as follows: elastic conditions, a coefficient of friction of  $\mu = 0.3$ , the same normal loads ( $P$  ranging from 100 N to 5000 N), and the same oscillation amplitude  $\Delta = 6 \mu\text{m}$  based on Eq. (29). The wear volume on the hemisphere for Inconel 617/Inconel 617 is slightly smaller than that for Inconel 617/Incoloy 800H because the nominal sliding distance at the initiation of gross slip is slightly larger for Inconel 617/Inconel 617 case. That can be understood because the larger nominal sliding distance at the initiation of gross slip,  $\delta_i$ , leads to smaller nominal sliding distance of gross slip,  $\Delta - \delta_i$ , which then results in the smaller wear volume. The wear volume on the block for Inconel 617/Inconel 617 is apparently smaller than that for Inconel 617/Incoloy 800H, because the hardness of Incoloy 800H is much smaller than that of Inconel 617. Therefore, the wear volume for Inconel 617/Inconel 617 case is smaller than that for Inconel 617/Incoloy 800H under the same fretting loading parameters. The wear volume maximizes at a certain load (about 5000 N) but drops after that because a higher load leads to a larger stick region, which lowers the wear volume. To summarize, from a practical point of view for the material pairs considered here, it is reasonable to choose Inconel 617/Inconel 617 as the contact pair to minimize wear damage. Note that the assumption in Fig. 7 is that the contact is entirely elastic. That is true for Inconel 617 (see Table 2,  $P_c = 13,472$  N). However, the contact of Incoloy

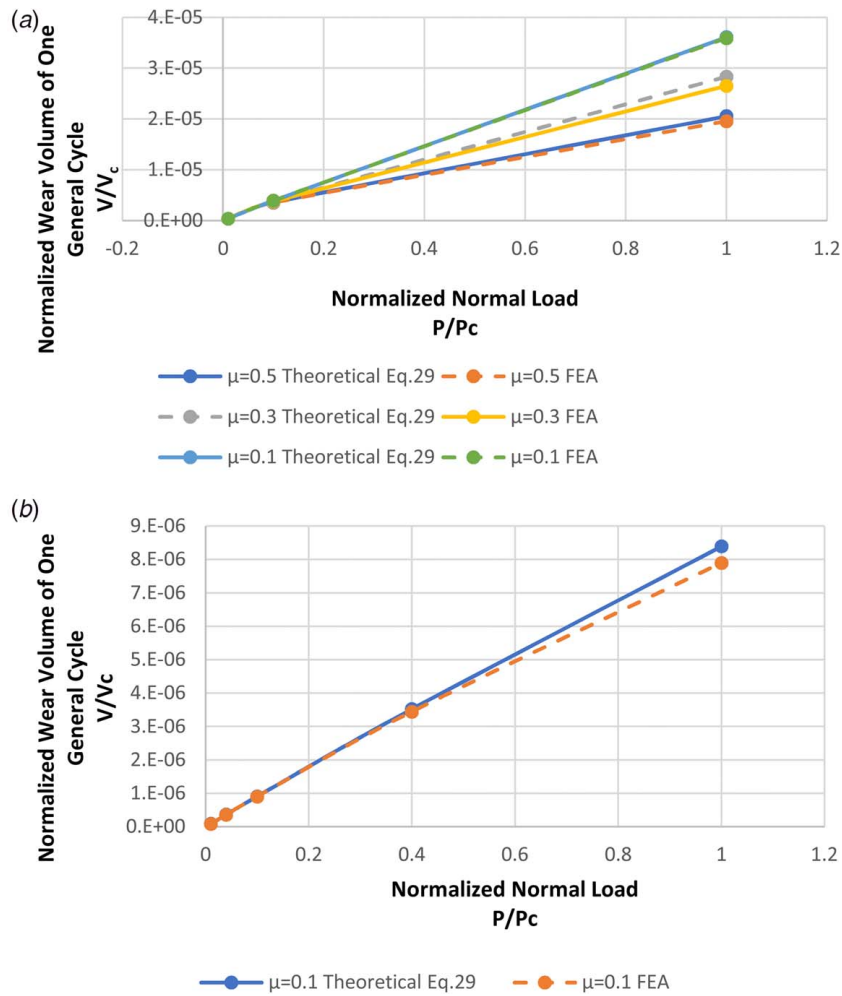


Fig. 6 The normalized wear volume for a general cycle of fretting motion at elastic condition with (a)  $\mu = 0.1, 0.3, \text{ and } 0.5$  (top to bottom curves, respectively) under different normal loads from FEA and theoretical predictions (Eq. (29)) for Inconel 617/Inconel 617 and (b)  $\mu = 0.1$  under different normal loads from FEA and theoretical predictions (Eq. (29)) for Inconel 617/Incoloy 800H

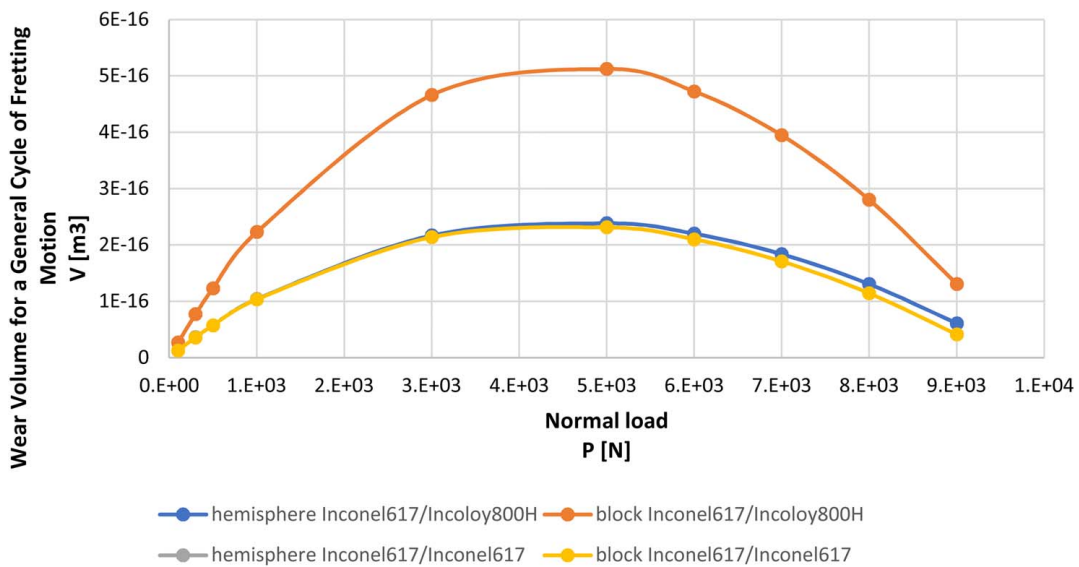
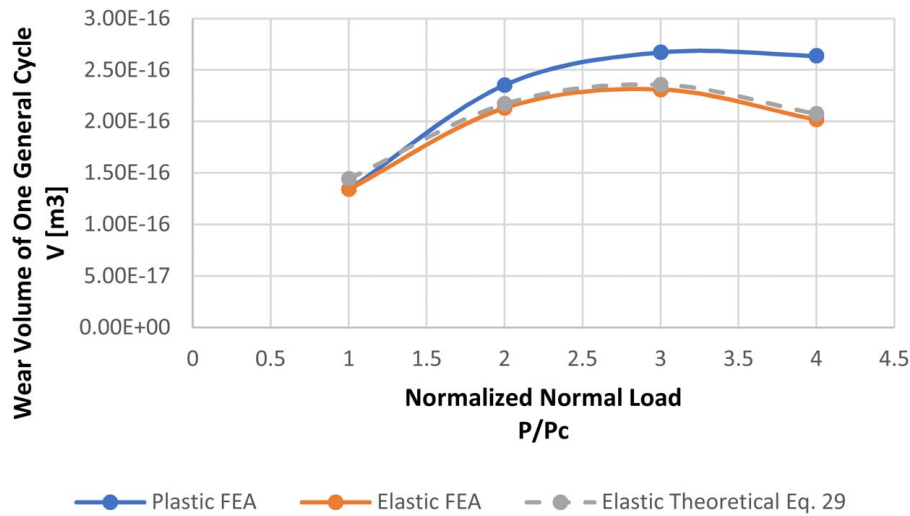


Fig. 7 The wear volumes on the hemisphere and the block for a general cycle of fretting motion at the elastic condition for  $\mu = 0.3$  under different normal loads from Eq. (29) for Inconel 617/Incoloy 800H and Inconel 617/Inconel 617



**Fig. 8** The wear volume for a general cycle of fretting motion at elastic and plastic conditions for  $\mu = 0.3$  under different normal loads from FEA and theoretical elastic predictions (Eq. (29)) for Inconel 617/Incoloy 800H

800H becomes plastic (at  $P_c = 1556$  N) based on the data in Table 2. The wear volume for Incoloy 800H would therefore be slightly higher than that shown in Fig. 7, where plasticity is investigated in Sec. 4.

#### 4 The Effect of Plasticity

The aforementioned results are obtained solely for pure elastic conditions. To find the influence of plasticity, an elastic-perfectly plastic material behavior condition is now numerically applied to both hemisphere and block. The wear volumes between the pure elastic regime and elastic-perfectly plastic regime are then contrasted under identical loading conditions. For the purely elastic regime, yielding is of course moot, allowing the elastic modulus to prevail throughout.

Figure 8 shows the wear volume of one general cycle of fretting motion at elastic and elastic-plastic conditions for  $\mu = 0.3$  under different normal loads for dissimilar material pair Inconel 617/Incoloy 800H. The elastic prediction agrees well with the FEA results under the said elastic conditions, while the results under elastic-plastic conditions are larger than the results under the purely elastic conditions. The increase of the wear volume under elastic-plastic conditions is due to the junction growth effect, which increases the contact area. However, the results between the elastic conditions and elastic-plastic conditions are still quite close to each other.

#### 5 Conclusion

A fretting wear model for spherical contact is built, and it is solved analytically. The wear model chosen at the interface of contact is that by Archard along with constant coefficients of friction. The analytical solutions for the nominal sliding distance at the initiation of gross slip, the wear volume at the initiation of gross slip, and the wear volume during early progression for one general cycle of fretting motion are derived for the purely elastic regime. The analytical solutions results are subsequently contrasted numerically to those obtained by the finite element method. The very good agreements for all of the results authenticate both the analytical derivations and the FEA model. In addition, the elastic-plastic contact conditions are also analyzed, and its effects on the wear volume during early progression is investigated. The junction growth effect increases the wear volume in the elastic-plastic conditions compared to that in purely elastic conditions. All results herein are presented in normalized forms. The dimensionless

results along with the analytical expressions can be easily generalized and applied to different material pairs.

#### Acknowledgment

This research is supported by the Department of Energy under Project 2506U87, Award RH452. This support is gratefully acknowledged.

#### Conflict of Interest

There are no conflicts of interest.

#### Nomenclature

- $a$  = contact radius, m
- $c$  = stick contact radius, m
- $q$  = tangential traction,  $q = q' + q''$ ,  $N/m^2$
- $s$  = local interfacial sliding distance, m
- $v$  = local wear volume,  $m^3$
- $C$  = Poisson's ratio parameter
- $E$  = elastic modulus,  $N/m^2$
- $G$  = shear modulus,  $N/m^2$
- $H$  = material hardness,  $N/m^2$
- $K$  = dimensionless wear coefficient
- $P$  = normal load, N
- $Q$  = tangential force, N
- $R$  = radius of hemisphere, m
- $S$  = sliding distance in Archard wear model, m
- $V$  = wear volume,  $m^3$
- $\bar{u}$  = tangential displacement on the surface of a half elastic space, m
- $a_c$  = critical contact radius, m
- $p_0$  = maximum contact pressure,  $N/m^2$
- $s_0$  = local interfacial sliding distance at the initiation of the gross slip, m
- $s_x$  = local interfacial sliding distance in X-direction, m
- $E_1$  = elastic modulus of the hemisphere,  $N/m^2$
- $E_2$  = elastic modulus of the block,  $N/m^2$
- $P_c$  = critical normal load, N
- $S_y$  = yield strength,  $N/m^2$
- $V_0$  = wear volume at the initiation of the gross slip,  $m^3$
- $V_c$  = critical wear volume,  $m^3$
- $q'$  = tangential traction at slip region,  $\mu p(r)$ ,  $N/m^2$

$q''$  = supplementary tangential traction at stick region, N/m<sup>2</sup>  
 $E'$  = equivalent elastic modulus, N/m<sup>2</sup>  
 $\delta$  = nominal sliding distance, m  
 $\delta_i$  = nominal sliding distance at the initiation of gross slip, m  
 $\delta_{i1}$  = the deformation of the stick region on hemisphere at the initiation of the gross slip, m  
 $\delta_{i2}$  = the deformation of the stick region on block at the initiation of the gross slip, m  
 $\Delta$  = oscillation amplitude of the fretting motion, m  
 $\mu$  = coefficient of friction  
 $\nu_1$  = Poisson's ratio of the hemisphere  
 $\nu_2$  = Poisson's ratio of the block  
 $\omega$  = interference, m  
 $\omega_c$  = critical interference, m

## References

- [1] Johnson, K. L., 1987, *Contact Mechanics*, Cambridge University Press, Cambridge, UK.
- [2] Tomlinson, G., Thorpe, P., and Gough, H., 1939, "An Investigation of the Fretting Corrosion of Closely Fitting Surfaces," *Proc. Inst. Mech. Eng.*, **141**(1), pp. 223–249.
- [3] Vingsbo, O., and Söderberg, S., 1988, "On Fretting Maps," *Wear*, **126**(2), pp. 131–147.
- [4] Zhou, Z., and Vincent, L., 1995, "Mixed Fretting Regime," *Wear*, **181**, pp. 531–536.
- [5] Zhou, Z., Nakazawa, K., Zhu, M., Maruyama, N., Kapsa, P., and Vincent, L., 2006, "Progress in Fretting Maps," *Tribol. Int.*, **39**(10), pp. 1068–1073.
- [6] Waterhouse, R., 1984, "Fretting Wear," *Wear*, **100**(1–3), pp. 107–118.
- [7] McColl, I., Ding, J., and Leen, S., 2004, "Finite Element Simulation and Experimental Validation of Fretting Wear," *Wear*, **256**(11–12), pp. 1114–1127.
- [8] Fouvry, S., Kapsa, P., Zahouani, H., and Vincent, L., 1997, "Wear Analysis in Fretting of Hard Coatings Through a Dissipated Energy Concept," *Wear*, **203**, pp. 393–403.
- [9] Blanchard, P., Colombie, C., Pellerin, V., Fayeulle, S., and Vincent, L., 1991, "Material Effects in Fretting Wear: Application to Iron, Titanium, and Aluminum Alloys," *Metall. Trans. A*, **22**(7), pp. 1535–1544.
- [10] Ding, J., Leen, S., and McColl, I., 2004, "The Effect of Slip Regime on Fretting Wear-Induced Stress Evolution," *Int. J. Fatigue*, **26**(5), pp. 521–531.
- [11] Ratsimba, C., McColl, I., Williams, E., Leen, S., and Soh, H., 2004, "Measurement, Analysis and Prediction of Fretting Wear Damage in a Representative Aeroengine Spline Coupling," *Wear*, **257**(11), pp. 1193–1206.
- [12] Fridrici, V., Fouvry, S., and Kapsa, P., 2003, "Fretting Wear Behavior of a Cu–Ni–In Plasma Coating," *Surf. Coat. Technol.*, **163**, pp. 429–434.
- [13] Paulin, C., Fouvry, S., and Meunier, C., 2008, "Finite Element Modelling of Fretting Wear Surface Evolution: Application to a Ti–6Al–4 V Contact," *Wear*, **264**(1–2), pp. 26–36.
- [14] Kogut, L., and Etsion, I., 2002, "Elastic–Plastic Contact Analysis of a Sphere and a Rigid Flat," *ASME J. Appl. Mech.*, **69**(5), pp. 657–662.
- [15] Jackson, R. L., and Green, I., 2005, "A Finite Element Study of Elasto-Plastic Hemispherical Contact Against a Rigid Flat," *ASME J. Tribol.*, **127**(2), pp. 343–354.
- [16] Tsukizoe, T., and Hisakado, T., 1968, "On the Mechanism of Contact Between Metal Surfaces: Part 2—The Real Area and the Number of the Contact Points," *ASME J. Lubr. Tech.*, **90**(1), pp. 81–88.
- [17] Green, I., 2005, "Poisson Ratio Effects and Critical Valus in Spherical and Cylindrical Hertzian Contacts," *Appl. Mech. Eng.*, **10**(3), p. 451.
- [18] Yang, H., and Green, I., 2018, "An Elastoplastic Finite Element Study of Displacement-Controlled Fretting in a Plane-Strain Cylindrical Contact," *ASME J. Tribol.*, **140**(4), p. 041401.
- [19] Yang, H., and Green, I., 2019, "A Fretting Finite Element Investigation of a Plane-Strain Cylindrical Contact of Inconel 617/Incoloy 800H at Room and High Temperatures," *Proc. Inst. Mech. Eng. Part J: J. Eng. Tribol.*, **233**(4), pp. 553–569.
- [20] Yang, H., and Green, I., 2019, "Analysis of Displacement-Controlled Fretting Between a Hemisphere and a Flat Block in Elasto-Plastic Contacts," *ASME J. Tribol.*, **141**(3), p. 031401.
- [21] Yang, H., and Green, I., 2019, "Fretting Wear Modeling of Cylindrical Line Contact in Plane-Strain Borne by the Finite Element Method," *ASME J. Appl. Mech.*, **86**(6), p. 061012.
- [22] METALS, S., 2008, "Product Handbook of Highperformance Nickel Alloys," Product Handbook.
- [23] Archard, J., 1953, "Contact and Rubbing of Flat Surfaces," *J. Appl. Phys.*, **24**(8), pp. 981–988.